Research Square

Preprints are preliminary reports that have not undergone peer review.
They should not be considered conclusive, used to inform clinical practice,
or referenced by the media as validated information.

An SO(3)-equivariant reciprocal space neural potential for long-range interactions

Taoyong Cui

cty21@tsinghua.org.cn

The Chinese University of Hong Kong https://orcid.org/0000-0002-5532-6636

Lingfeng Zhang

The Hong Kong Polytechnic University, Department of Electrical and Electronic Engineering

Dongzhan Zhou

Shanghai Artificial Intelligence Laboratory https://orcid.org/0000-0001-6568-5440

Lei Bai

Shanghai AI Laboratory https://orcid.org/0000-0003-3378-7201

Shufei Zhang

Shanghai Artificial Intelligence Laboratory https://orcid.org/0000-0002-4614-4718

Luca Rossi

The Hong Kong Polytechnic University

Mao Su

Shanghai Artificial Intelligence Laboratory https://orcid.org/0000-0003-2066-881X

Wanli Ouyang

Shanghai Artificial Intelligence Laboratory

Pheng Ann Heng

The Chinese University of Hong Kong https://orcid.org/0000-0003-3055-5034

Article

Keywords: Machine Learning Interatomic Potentials, Long Range Dependence, Graph Neural Network

Posted Date: August 3rd, 2026

DOI: https://doi.org/10.21203/rs.3.rs-10489824/v1

License: This work is licensed under a Creative Commons Attribution 4.0 International License.
Read Full License

Additional Declarations: There is **NO** Competing Interest.

An SO(3)-equivariant reciprocal space neural potential for long-range interactions

Lingfeng Zhang[1,3†], Taoyong Cui[1†], Dongzhan Zhou[2], Lei Bai[2], Shufei Zhang[2], Luca Rossi[3*], Mao Su[2,4*], Wanli Ouyang[1,2*], Pheng-Ann Heng[1]

[1]The Chinese University of Hong Kong, Hong Kong, 999077, China.
[2]Shanghai Artificial Intelligence Laboratory, Shanghai, 200232, China.
[3]Department of Electrical and Electronic Engineering, The Hong Kong Polytechnic University, Hong Kong, 999077, China.
[4]Shenzhen Institute of Advanced Technology, Chinese Academy of Sciences, Shenzhen, 518055, China.

*Corresponding author(s). E-mail(s): luca.rossi@polyu.edu.hk; sumao@pjlab.org.cn; wlouyang@ie.cuhk.edu.hk;
†These authors contributed equally to this work.

Abstract

Long-range electrostatic and polarization interactions play an essential role in molecular and condensed-phase systems but remain challenging for machine-learning interatomic potentials based on local atomic environments. Although SO(3)-equivariant neural potentials can learn rich representations of local geometry, atoms or molecular fragments separated by more than the real-space cutoff do not communicate directly. We introduce EquiEwald, a neural interatomic potential that extends Ewald summation to operate directly on SO(3)-equivariant tensor features rather than scalar, charge-like information. This allows reciprocal-space communication to preserve orientation-dependent information across arbitrary distances while maintaining rotational symmetry. Across periodic and aperiodic benchmarks, EquiEwald captures long-range electrostatic behavior consistent with ab initio reference data and consistently improves energy and force accuracy, data efficiency, and long-range extrapolation. These results establish EquiEwald as a physically motivated framework for incorporating long-range interactions in machine-learning interatomic potentials.

Keywords: Machine Learning Interatomic Potentials, Long Range Dependence, Graph Neural Network

1 Introduction

Molecular dynamics (MD) simulations are widely used to investigate atomistic processes in chemical, materials, and biological systems [1–5]. Despite decades of progress, achieving quantum-level accuracy at the spatial and temporal scales required for realistic materials and molecular systems remains a central challenge. Quantum-mechanical methods such as density functional theory (DFT) deliver reliable energies and forces [6], but their steep computational cost restricts system sizes and timescales. Classical force fields, while efficient, often lack the transferability and predictive fidelity needed for complex chemistries [7]. Machine-learning interatomic potentials (MLIPs) provide an intermediate approach by learning high-dimensional potential-energy surfaces from *ab initio* reference data [8–11]. They can substantially reduce the cost of energy and force evaluations while retaining reference-level accuracy within the configurational domain represented by the training data [12].

Within this landscape, SO(3)-equivariant graph neural networks, including NequIP [13], Allegro [14], and MACE [15], have emerged as state-of-the-art short-range MLIPs. By explicitly encoding rotational and translational symmetries, these models can improve data efficiency and robustness across chemical space. Many widely used equivariant MLIPs construct atomic representations from neighborhoods defined by a finite real-space cutoff. Unless information is propagated through sufficiently many layers or supplemented by a global pathway, fragments separated beyond the effective receptive field cannot communicate directly [16–18]. This assumption becomes limiting in systems where important contributions arise from long-range electrostatics which decay slowly and may exhibit pronounced anisotropy [19–21]. As a result, even highly expressive equivariant architectures can struggle when long-range interactions depend on the spatial arrangement and relative orientation of distant parts of the system [16, 22–24]. The underlying issue is a mismatch between the nonlocal nature of these interactions and architectures that exchange information mainly within finite real-space neighborhoods.

Efforts to incorporate long-range interactions into MLIPs have continued for years. Early work extended short-range models with empirical electrostatics and dispersion baselines, which enforce the correct asymptotic behavior but are typically system-dependent and hard to obtain for complex, heterogeneous environments [25, 26]. A more general line of work learns intermediate physical surrogates, most commonly effective partial charges or electronic proxies such as Wannier-center-based representations, and then evaluates long-range electrostatics explicitly [27–31]. These approaches are easier to interpret and can capture polarization effects, but they often require additional supervision and remain sensitive to the non-uniqueness of charge partitioning. Message-passing models [13, 32, 33] extend the receptive field by stacking local convolutions, yet truly nonlocal couplings, such as interactions between fragments separated beyond the cutoff, are still difficult to capture. Inspired by Ewald summation, more recent work models long-range effects in Fourier space by aggregating global interactions through Fourier components with learnable frequency filters [34–36]. These methods replace real-space distance truncation with low-frequency global communication and provide an effective augmentation to local message-passing architectures. However, these frameworks encode reciprocal space signals using scalar

structure factors or latent charge-like variables, which average over angular information and can limit the description of directional electrostatics, multipolar correlations, and anisotropic polarization. LODE methods [24, 37] provide a complementary strategy by using local descriptors to parameterize Coulomb and more general $1/r^p$ far-field interactions. This formulation preserves analytic asymptotic behavior and enables the incorporation of physically motivated long-range terms within equivariant frameworks. However, because the long-range contributions are introduced through predefined functional forms, these approaches can be less flexible in capturing complex environment-dependent electronic correlations, and they do not fully integrate long-range interactions into a unified end-to-end learning architecture.

Here, we introduce **EquiEwald**, a unified SO(3)-equivariant neural interatomic potential that embeds Ewald summation within an irreducible representation framework [38]. EquiEwald replaces the conventional locality assumption with a degree-resolved Fourier space pathway that enables long-range interactions to be represented at the tensorial level. By propagating degree-resolved SO(3)-equivariant latent features through Fourier space, EquiEwald couples spatially separated atomic environments while retaining the angular information encoded by different irreducible-representation channels. Specifically, EquiEwald computes irreducible representation-resolved structure factors, applies learned k-space filters under both periodic and aperiodic boundary conditions, and maps spectral signals back to atomic space through an equivariant inverse transform, yielding a unified treatment of real-space and reciprocal space physics within a single differentiable architecture. Across a suite of demanding benchmarks, we show that this representation-level integration of reciprocal space information leads to improved accuracy, data efficiency, and transferability in systems governed by nonlocal interactions. EquiEwald provides a physically structured, equivariant framework for learning long-range interactions directly from *ab initio* data, addressing a fundamental representational limitation of locality-based MLIPs.

2 Results

2.1 Preliminaries

Machine-learning interatomic potentials (MLIPs) learn a mapping from an atomic structure to its total energy E, with atomic forces obtained as

$$\mathbf{F}_i = -\nabla_{\mathbf{r}_i} E. \tag{1}$$

In the absence of external fields, the total energy is invariant under global translations and rotations, as well as permutations of atoms of the same species, while the predicted forces transform covariantly under rotations. Modern neural potentials incorporate these symmetries into their architectures to improve physical consistency and generalization [13, 14].

In this work, atomic features are organized into irreducible representations of SO(3) indexed by the spherical degree ℓ [39, 40]. The $\ell = 0$ features are rotationally invariant scalars, whereas features with $\ell > 0$ retain orientation-dependent information and transform equivariantly under global rotations. This degree-resolved representation

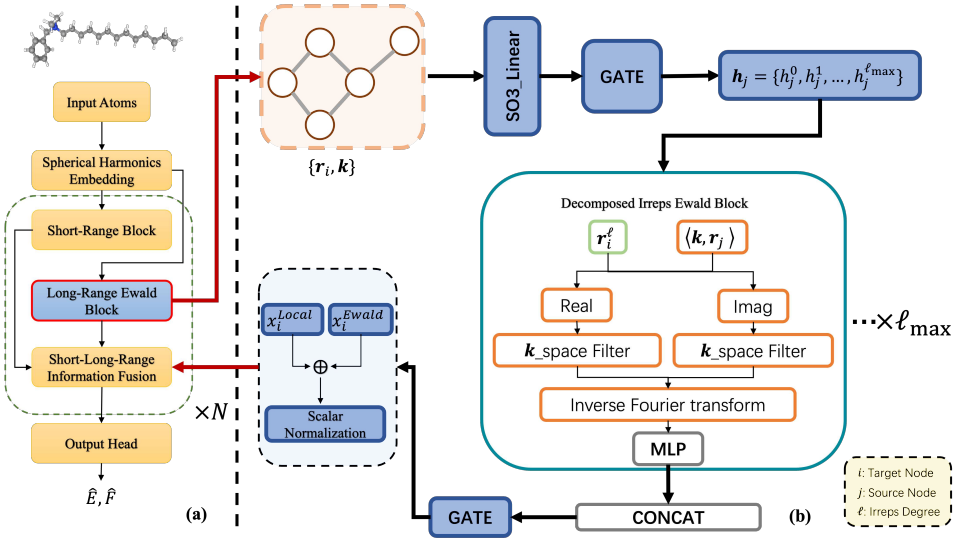


Fig. 1: **Overview. a**, The model architecture of EquiEwald. **b**, The EquiEwald long-range block takes node features and wave-vector inputs, applies an SO(3) linear map and gating, then decomposes degree-ℓ irreducible representation into real/imag branches with k-space filters driven by $\langle \mathbf{k}, \mathbf{r}_j \rangle$; an inverse Fourier transform and an MLP return real-space updates per degree. Outputs across degrees are concatenated and gated, then fused with normalized local features to yield a rotationally equivariant long-range interaction update.

provides the basis for propagating both scalar and directional information through the model.

EquiEwald extends this representation to Fourier space communication. It processes each irreducible degree separately through Fourier aggregation, frequency-domain filtering, and inverse accumulation, while preserving the corresponding SO(3) transformation properties. The complete mathematical formulation and equivariance analysis are provided in the Methods and Supplementary Information.

2.2 Overall structure of EquiEwald

EquiEwald is a neural framework for learning interatomic potentials that unifies short-range geometric modeling with long-range physical interactions in a single, rotation-equivariant architecture. As shown in Fig. 1(a), it consists of two representation pathways: a short-range encoder that captures local atomic environments using a local graph message passing backbone, and a long-range spectral encoder that introduces nonlocal information via message passing in Fourier space. Both components operate on the same atom-wise input and their outputs are fused through a residual update to form the final atomic representation used for energy and force prediction.

A central feature of EquiEwald, illustrated in Fig. 1(b), is that non-scalar features are not reduced to invariant summaries before Fourier space communication. Instead, each degree is propagated with the same channel operation across its m components. The Fourier phase is a scalar under simultaneous rotation of positions and wave vectors, so this construction can retain orientation-dependent nonlocal information without changing the transformation type of the feature. By embedding a Fourier space communication structure into the representation space, EquiEwald provides a unified framework of short-range and long-range physics effects.

2.3 Experimental results

The effectiveness of EquiEwald was systematically evaluated on both aperiodic and periodic systems, including charged dimers, biomolecular dynamics, molten ionic systems, and periodic catalytic interfaces. For the main results, we adopted the eSCN framework [41] as our primary method. For periodic systems, we additionally included EquiformerV2 [42] as another baseline. Aperiodic benchmarks included molecular dimer [36], and AIMD-Chig [43], while periodic systems were assessed using molten NaCl [44] and the OC20 dataset [45]. For the OC20 dataset, we additionally evaluated EquiEwald using the EquiformerV2 [42] backbone.

Molecular Dimers. We evaluate the EquiEwald blocks on selected dimer systems formed from charged (C), polar (P), and apolar (A) molecules at intermolecular separations of approximately 5-15 Å. In Fig. 2, the representative molecular conformations are shown in the top row, and the corresponding binding energy curves are reported for four dimer classes: CC, CA, CP, and PP. The middle row shows the results of the short-range eSCN base model, while the bottom row shows the eSCN with long-range EquiEwald blocks. For each system, solid curves denote training samples and dashed curves denote test samples, with reference energies shown in blue and model predictions in red. The short-range model shows clear deviations from the reference binding curves, particularly for the CC and CP systems, where the predicted curves flatten and fail to reproduce the long-range decay. In contrast, the long-range model closely follows the reference curves over both the training and testing distances. Quantitatively, the total energy MAE is reduced from 363.89 to 9.41 meV for CC, from 4.49 to 2.29 meV for CA, from 140.61 to 13.92 meV for CP, and from 5.61 to 1.91 meV for PP.

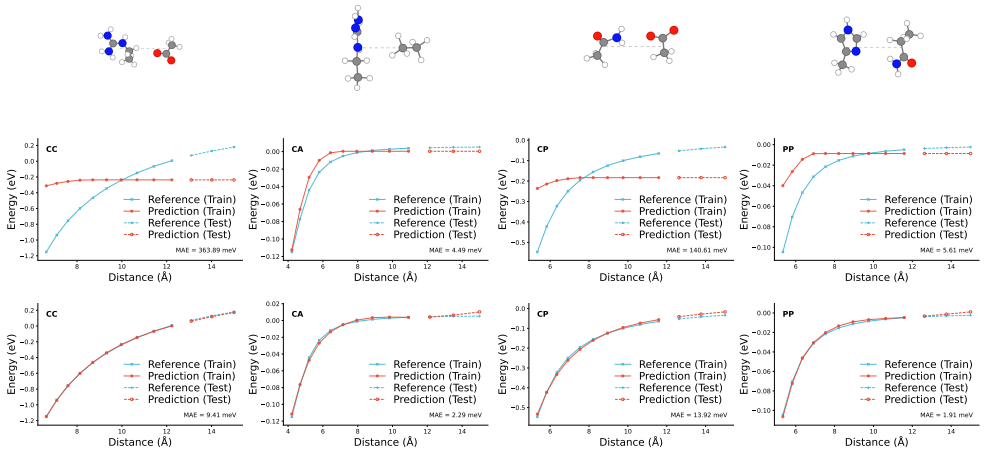


Fig. 2: **Benchmark comparison between short-range and long-range models on molecular dimer systems.** Comparison of the binding energy curves for the eSCN baseline and eSCN + EquiEwald across four dimer classes: charged-charged (CC), charged-apolar (CA), charged-polar (CP), and polar-polar (PP). The top row shows conformations of the four dimer systems. The middle row presents the binding energy curves predicted by the short-range eSCN model, while the bottom row presents the corresponding results from the long-range eSCN + EquiEwald model. The binding energy is defined as the potential energy difference between the dimer and its isolated monomers. Each panel reports the energy MAE of the corresponding model.

AIMD-Chig. Derived from ab initio molecular dynamics of the protein Chignolin, AIMD-Chig poses challenges due to its flexible backbone, complex conformational dynamics, and long-range intramolecular interactions that are important for maintaining structural stability. As shown in Table 1, the baseline eSCN model yields a test energy MAE of 193.9 meV and a force MAE of 23.1 meV/Å. Incorporating scalar EwaldMP improves both energy and force predictions, reducing the errors to 132.8 meV and 20.3 meV/Å, respectively. In contrast, LES gives a force MAE of 22.7 meV/Å with almost unchanged energy error compared with the eSCN baseline, while SOG-Net achieves a lower force MAE than eSCN but does not improve the energy prediction on this dataset. With EquiEwald, the errors are further reduced to 109.0 meV and 18.1 meV/Å, corresponding to improvements of 44% and 21% over the eSCN baseline, respectively. These results suggest that reciprocal space information with angular resolution provides additional representational capacity for modeling collective motions and long-range electrostatics in biomolecular systems.

We further evaluate whether thermodynamic properties predicted by explicitly modeling long-range interactions are consistent with experimental observations using the fast-folding protein Chignolin. From the simulation trajectories, 100,000 conformational snapshots were uniformly sampled and analyzed using the Q score, which measures the fraction of native contacts relative to the reference folded structure. The

Table 1: Performance comparison of different long-range interaction modeling approaches on the AIMD-Chig dataset. The baseline eSCN model is compared with methods incorporating scalar EwaldMP, LES, SOG-Net, and the proposed EquiEwald method. Mean Absolute Errors (MAE) for energy and atomic forces are reported in **meV** and **meV/Å**, respectively, while the folding free-energy difference (ΔG) is reported in **meV** to maintain consistency with thermodynamic conventions.

Model	Test Energy (MAE)	Test Force (MAE)	ΔG (MAE)
eSCN [41]	193.9	23.1	49.9
eSCN+EwaldMP [35]	132.8	20.3	37.7
eSCN+LES [36]	193.8	22.7	39.9
eSCN+SOG-Net [46]	205.9	22.8	38.6
eSCN + EquiEwald	**109.0**	**18.1**	**29.1**

model-predicted potential energies were then used to reconstruct the energy landscape and estimate thermodynamic quantities, including the folding free-energy difference (ΔG), using the computational protocols exactly as described in [47]. Compared to the baseline eSCN model, which relies solely on local message passing, incorporating the EquiEwald reciprocal space module substantially improves the accuracy of energy predictions relevant to free-energy estimation. Specifically, the prediction error is reduced from 49.9 meV for eSCN to 29.1 meV for eSCN + EquiEwald, corresponding to an approximate 41.7% relative reduction. This improvement demonstrates that explicitly modeling long-range electrostatic interactions leads to more accurate thermodynamic estimates. In contrast, purely local representations struggle to capture the collective intramolecular interactions that stabilize folded conformations in Chignolin.

Molten NaCl. Molten sodium chloride is an ionic liquid in which Coulomb interactions extend well beyond typical local cutoffs. We evaluate EquiEwald on a molten NaCl benchmark containing $1,014$ structures, each with 64 Na and 64 Cl atoms, using an 80%/20% train–validation split. Energy errors are normalized per atom, whereas force errors are reported for atomic force components in meV/Å. Table 2 compares EquiEwald with the local eSCN baseline [41] and the EwaldMP [35], LES [36], and SOG-Net [46] long-range extensions.

The local eSCN model gives the largest errors, with an energy RMSE of 1.459 meV/atom and a force RMSE of 48.621 meV/Å. All four long-range extensions lower the energy and force errors, consistent with the importance of nonlocal interactions in molten NaCl. eSCN+LES gives the lowest force MAE, 9.494 meV/Å. eSCN + EquiEwald gives the lowest energy RMSE, energy MAE, and force RMSE, while its force MAE is the second lowest. Relative to eSCN, EquiEwald reduces the energy RMSE from 1.459 to 0.372 meV/atom (74.5%) and the force RMSE from 48.621 to 14.054 meV/Å (71.1%).

OC20. We further evaluate EquiEwald on the OC20 structure to energy and forces (S2EF) task, which contains catalyst surface–adsorbate structures in periodic simulation cells. As shown in Table 3, adding EquiEwald improves both backbones. Because

Table 2: Energy and force errors on molten NaCl. Energy errors are reported in **meV/atom**, and force-component errors are reported in **meV/Å**. RMSE and MAE denote root-mean-square error and mean absolute error, respectively. The best result for each metric is shown in bold.

Model	Energy RMSE (meV/atom)	Energy MAE (meV/atom)	Force RMSE (meV/Å)	Force MAE (meV/Å)
eSCN [41]	1.459	1.212	48.621	37.859
eSCN+EwaldMP [35]	0.474	0.387	22.607	16.614
eSCN+LES [36]	0.569	0.496	15.174	**9.494**
eSCN+SOG-Net [46]	0.514	0.432	19.855	14.310
eSCN + EquiEwald	**0.372**	**0.321**	**14.054**	10.528

Table 3: Mean absolute errors (MAE) of energy and force. Results are reported on the evaluation splits for OC20. Energy errors are reported in **meV**, and force errors are in **meV/Å**. Our method is highlighted in bold.

Model	Energy MAE (meV)	Force MAE (meV Å^{-1})
eSCN [41]	347.0	24.7
eSCN + EquiEwald	**321.2**	**24.1**
EquiformerV2 [42]	541.0	46.4
EquiformerV2+EquiEwald	**453.0**	**38.4**

training on OC20 needs substantial computational cost, we limit OC20 evaluation to eSCN and EquiformerV2, comparing each model with and without the EquiEwald module. For eSCN, EquiEwald reduces the energy MAE from 347.0 to 321.2 meV. The force MAE decreases from 24.7 to 24.1 meV/Å. EquiEwald yields a more pronounced improvement in energy prediction than in force prediction, which is consistent with the analysis reported in EwaldMP [35]. For a Fourier component with wave vector $\mathbf{k}$, differentiation with respect to an atomic coordinate introduces a factor of $i\mathbf{k}$, such that the magnitude of the corresponding force contribution is weighted by $\|\mathbf{k}\|$. Consequently, the low-frequencies retained by the reciprocal-space branch contribute less strongly to the energy gradient than higher-frequencies. The magnitude of the improvement also depends on the backbone employed. We incorporated EquiEwald into EquiformerV2 and observed better improvements in both energy and force prediction: the energy MAE decreased from 541.0 to 453.0 meV, while the force MAE decreased from 46.4 to 38.4 meV/Å.

2.4 Computational efficiency

We evaluated the computational cost by measuring the average inference time per structure on the OC20 evaluation dataset. All measurements were performed on NVIDIA GeForce RTX 4090 GPUs using the same inference settings. The baseline eSCN model requires 2.8 ms per structure, while eSCN + EquiEwald takes 4.8 ms.

The eSCN + EwaldMP variant requires 4.4 ms per structure. Thus, introducing long-range Fourier space communication increases the inference time by approximately 2.0 ms relative to the short-range baseline, while retaining millisecond-level inference efficiency.

The additional cost primarily arises from the forward and inverse Fourier accumulations. Let N_{at} denote the number of atoms and N_k the number of sampled Fourier modes. Suppressing the fixed feature dimensions, the computational complexity of the EquiEwald update is $\mathcal{O}(N_{\mathrm{at}}N_k)$. The local message-passing backbone scales as $\mathcal{O}(N_{\mathrm{at}}\bar{n})$, where $\bar{n}$ is the average number of neighbors within the real-space cutoff. The resulting complexity of the combined model is therefore

$$\mathcal{O}(N_{\mathrm{at}}\bar{n} + N_{\mathrm{at}}N_k)\,. \tag{2}$$

For fixed real-space and Fourier space sampling settings, both $\bar{n}$ and N_k remain bounded, giving approximately linear scaling with the number of atoms. EquiEwald therefore enables global communication without constructing an explicit fully connected atom-pair graph, which would incur $\mathcal{O}(N_{\mathrm{at}}^2)$ complexity.

3 Discussion

In this work, we introduced EquiEwald, an SO(3)-equivariant neural interatomic potential that augments local message passing with degree-resolved Fourier space communication. The construction retains the nonlocal structure factor factorization of EwaldMP while extending the Fourier space branch from invariant scalar embeddings to features spanning multiple irreducible degrees. Across the molecular-dimer, AIMD-Chig, molten NaCl, and OC20 benchmarks, EquiEwald improves energy and force prediction relative to the corresponding local backbone. The dimer results additionally show improved extrapolation to fragment separations beyond the local cutoff. These observations support the value of propagating orientation-dependent latent information through a global low-frequency pathway.

A key implication of this work is that incorporating long-range interactions into neural potentials is not only a problem of extending spatial receptive fields, but also a problem of preserving the geometric structure of learned representations during nonlocal communication. Classical Ewald summation decomposes slowly decaying interactions into real-space and Fourier space contributions, where the reciprocal component captures global spatial correlations through Fourier representations. EquiEwald extends this principle from scalar physical quantities to learned equivariant features by constructing degree-resolved structure factors and propagating each irreducible representation through Fourier space. This enables long-range communication while retaining angular information associated with higher-order SO(3) features, providing a learned analogue of multipolar representations used in traditional electrostatic models.

A central advantage of EquiEwald is that higher-degree information generated by the local equivariant encoder remains available during long-range communication. In scalar EwaldMP, the Fourier space pathway aggregates invariant channels and therefore communicates global information without retaining an explicit degree-resolved

transformation structure. EquiEwald instead constructs structure factor embeddings separately for each degree ℓ and applies channel operations consistently across the corresponding m components. The $\ell = 0$ channels communicate invariant information, whereas the $\ell > 0$ channels allow the long-range update to remain sensitive to the relative orientation of spatially separated environments. In this way, the model can distinguish nonlocal configurations that may have similar scalar summaries but differ in their directional organization.

The magnitude of improvement also reflects the physical characteristics of different systems. EquiEwald provides the gains for systems where long-range electrostatics strongly influence the energy landscape, where local cutoff-based representations cannot directly capture slowly decaying interactions. For complex biomolecular systems such as Chignolin, the improvement in energy prediction and thermodynamic estimation suggests that Fourier space features contribute to modeling collective intramolecular interactions beyond pairwise local environments.

This combination of local equivariant encoding and degree-resolved global communication provides a general framework for neural potentials in systems where important correlations extend beyond conventional real-space cutoffs. One limitation of the current implementation concerns aperiodic systems. As detailed in Methods section, the reciprocal lattice co-rotates with the cell and atomic coordinates in periodic systems, preserving the intended SO(3) transformation properties. In aperiodic systems, however, Fourier space is represented by a finite Cartesian grid that is not closed under arbitrary three-dimensional rotations. The resulting implementation therefore provides a resolution-dependent approximation to the continuous SO(3)-equivariant operator. Future work could quantify and reduce this discretization error using adaptive, higher-resolution, or rotation-compatible Fourier-space sampling schemes.

4 Methods

4.1 Model implementations

Short-range Encoder. To encode local short-range information, we use equivariant neural networks whose initial scalar features $\mathbf{x}_i^0$ are embeddings of the atomic number z_i. Relative displacement directions are expanded in spherical harmonics. The degree ℓ indexes angular frequency, and $m = -\ell, \ldots, \ell$ indexes the components that mix under rotations. Increasing ℓ_{max} increases the angular bandwidth of the representation; the body order represented by the network also depends on the number and form of its interaction layers and cannot be identified with ℓ alone. Equivariant operations iteratively update the atom features to produce the local representation. Details of the eSCN [41] and EquiformerV2 [42] backbones are provided in Supplementary Section 3.

Long-range Encoder. The EquiEwald block extends Ewald message passing (EwaldMP) [35] from scalar atom embeddings to features organized according to irreducible representations of SO(3). In the original EwaldMP formulation, Fourier space communication is performed using invariant scalar features. EquiEwald retains this global Fourier space communication mechanism but applies it separately to feature blocks of each irreducible degree ℓ, in a manner consistent with their corresponding

rotation transformation laws. This allows non-scalar information generated by the equivariant local encoder to participate directly in long-range communication without first being reduced to scalar summaries. By preserving the transformation structure of these features throughout Fourier space communication, EquiEwald broadens the symmetry representation space available for modeling nonlocal correlations.

EquiEwald follows the Fourier space communication mechanism of EwaldMP, but applies it to each equivariant feature degree separately. The operation consists of three steps: (i) summarize atom-wise features into Fourier space global descriptors, (ii) apply a learnable frequency filter, and (iii) map the filtered Fourier space features back to atom real space. This construction provides a global communication pathway in addition to cutoff-limited real-space message passing, allowing each atom to receive information from the entire structure through a finite set of sampled Fourier cutoff. We first recall the scalar construction used in EwaldMP [35]. A generic long-range message can be written as a convolution interaction

$$\mathbf{m}_i^{\mathrm{lr}} = \sum_{j\in\mathcal{S}} \Phi^{\mathrm{lr}}(\mathbf{r}_i - \mathbf{r}_j)\, \mathbf{h}_j, \tag{3}$$

where $\mathbf{m}_i^{\mathrm{lr}}$ denotes the long-range message received by atom i, $\mathcal{S}$ is the set of atoms in the structure or in the periodic supercell, j indexes a source atom, $\mathbf{r}_i, \mathbf{r}_j \in \mathbb{R}^3$ are atomic positions, $\mathbf{h}_j \in \mathbb{R}^C$ is the scalar embedding of atom j with C channels, and Φ^{lr} is a slowly varying long-range kernel. At this stage, both the atomic embeddings and the messages are real-valued. Instead of truncating this interaction in real space, EwaldMP represents the long-range kernel with a finite set of Fourier frequencies controlled by a frequency cutoff,

$$\Phi^{\mathrm{lr}}(\mathbf{r}_i - \mathbf{r}_j) \approx \sum_{\mathbf{k}\in\mathcal{K}} \exp\big(\mathrm{i}\,\mathbf{k}^\top(\mathbf{r}_i - \mathbf{r}_j)\big)\widehat{\Phi}^{\mathrm{lr}}(\mathbf{k}), \tag{4}$$

where $\mathbf{k} \in \mathbb{R}^3$ is a Fourier wave vector, $\mathcal{K}$ is the finite set of sampled wave vectors, $\widehat{\Phi}^{\mathrm{lr}}(\mathbf{k})$ is the learnable frequency filter at frequency $\mathbf{k}$, and $\mathrm{i} = \sqrt{-1}$ is the imaginary unit. The complex exponential introduces the complex-valued Fourier representation.

More explicitly, the forward Fourier accumulation produces the structure factor

$$\mathbf{s}(\mathbf{k}) = \sum_{j\in\mathcal{S}} \exp\big(-\mathrm{i}\,\mathbf{k}^\top\mathbf{r}_j\big)\mathbf{h}_j \in \mathbb{C}^C. \tag{5}$$

Thus, although the input embeddings $\mathbf{h}_j$ are real-valued, $\mathbf{s}(\mathbf{k})$ is generally complex-valued because of the Fourier phase. After frequency filtering, the message is mapped back to atom real space by

$$\mathbf{m}_i^{\mathrm{lr}} = \mathrm{Re}\sum_{\mathbf{k}\in\mathcal{K}} \exp\big(\mathrm{i}\,\mathbf{k}^\top\mathbf{r}_i\big)\widehat{\Phi}^{\mathrm{lr}}(\mathbf{k})\,\mathbf{s}(\mathbf{k}) \in \mathbb{R}^C. \tag{6}$$

The forward accumulation therefore maps real-valued atom features to complex-valued structure factor in Fourier space, whereas the inverse accumulation returns a real-valued atom-wise message. In implementation, the same operation is evaluated using

separate cosine and sine components rather than explicit complex-valued tensors. The EwaldMP formulation cannot be applied to non-scalar equivariant features directly. For $\ell > 0$, the $2\ell + 1$ feature components mix under rotation, so treating them as independent scalar channels or filtering them arbitrarily would generally break the corresponding SO(3) transformation law. EquiEwald addresses this issue by preserving the degree-wise feature structure and sharing the channel operation across all m components within each degree ℓ.

EquiEwald keeps this EwaldMP factorization but replaces scalar embeddings with irreducible SO(3) tensor features in long-range block. At layer t, the atom representation is decomposed into spherical harmonic degrees

$$\mathbf{x}_i^{(\ell)} = \big[\mathbf{x}_{i,m}^{(\ell)}\big]_{m=-\ell}^{\ell} \in \mathbb{R}^{(2\ell+1)\times C}, \qquad \ell = 0, \ldots, \ell_{\max}, \tag{7}$$

where t is the layer index, $\mathbf{x}_i^{(\ell)}$ is the degree-ℓ feature of atom i, $\ell_{\max}$ is the maximum spherical harmonic degree, $m = -\ell, \ldots, \ell$ indexes the $2\ell + 1$ coordinates within the degree-ℓ irreducible representation, and C is the number of channels per degree, so that each component $\mathbf{x}_{i,m}^{(\ell)} \in \mathbb{R}^C$ is a real C-channel vector. Under a rotation $R \in SO(3)$, these m components rotate into one another through the Wigner D-matrix $D^{(\ell)}(R)$. The $\ell = 0$ block carries invariant scalar information, whereas $\ell > 0$ blocks carry orientation-aware latent features. These higher-degree channels allow the learned long-range message itself to retain directional information.

For each degree ℓ and component m, EquiEwald first computes a degree-resolved structure factor,

$$\mathbf{s}_{\alpha,m}^{(\ell)} = \sum_{j\in\mathcal{S}} \omega_\Delta(\mathbf{k}_\alpha, \mathbf{r}_j) \exp\big(-\mathrm{i}\,\mathbf{k}_\alpha^\top \mathbf{r}_j\big)\mathbf{x}_{j,m}^{(\ell)}, \tag{8}$$

where $\mathbf{s}_{\alpha,m}^{(\ell)}$ is the complex-valued structure factor for degree ℓ, component m, and Fourier frequency index α; $\{\mathbf{k}_\alpha\}_{\alpha=1}^{N_k}$ are the retained Fourier frequencies; and N_k is the number of retained frequencies. The atom features $\mathbf{x}_{j,m}^{(\ell)}$ are real-valued, and the complex-valuedness of the structure factor arises solely from the Fourier phase $\exp\big(-\mathrm{i}\,\mathbf{k}_\alpha^\top \mathbf{r}_j\big)$. The scalar factor $\omega_\Delta(\mathbf{k}, \mathbf{r})$ denotes the sampling window associated with the chosen frequency discretization, where the subscript Δ refers to the reciprocal-grid resolution such as Δk in aperiodic systems. It equals one for periodic reciprocal lattice sampling and becomes a voxel-averaging window for aperiodic Cartesian grids.

The structure factors are then filtered in Fourier space,

$$\widetilde{\mathbf{s}}_{\alpha,m}^{(\ell)} = \mathbf{W}_\ell(\mathbf{k}_\alpha)\, \mathbf{s}_{\alpha,m}^{(\ell)}, \tag{9}$$

where $\widetilde{\mathbf{s}}_{\alpha,m}^{(\ell)}$ is the filtered structure factor and $\mathbf{W}_\ell(\mathbf{k}_\alpha) \in \mathbb{R}^{C\times C}$ is the learnable degree-ℓ channel filter at Fourier frequency $\mathbf{k}_\alpha$. The filtered signal is then mapped back to atom real space by the inverse Fourier accumulation

$$\mathbf{M}_{i,m}^{(\ell)} = \mathrm{Re} \sum_{\alpha=1}^{N_k} \omega_\Delta(\mathbf{k}_\alpha, \mathbf{r}_i) \exp\big(\mathrm{i}\,\mathbf{k}_\alpha^\top \mathbf{r}_i\big)\widetilde{\mathbf{s}}_{\alpha,m}^{(\ell)}. \tag{10}$$

Here $\mathbf{M}_{i,m}^{(\ell)} \in \mathbb{R}^C$ is the atom-space long-range message for atom i, degree ℓ, and component m, and Re takes the real part of the complex Fourier sum.

This operator is SO(3)-equivariant by construction. Under a global rotation R, positions and reciprocal vectors co-rotate as $\mathbf{r}_i \mapsto R\mathbf{r}_i$ and $\mathbf{k}_\alpha \mapsto R\mathbf{k}_\alpha$, while degree-$\ell$ features transform as $\mathbf{x}_i^{(\ell)} \mapsto D^{(\ell)}(R)\mathbf{x}_i^{(\ell)}$. The Fourier phase is invariant because

$$(R\mathbf{k}_\alpha)^\top (R\mathbf{r}_i) = \mathbf{k}_\alpha^\top \mathbf{r}_i. \tag{11}$$

Here R is an arbitrary three-dimensional rotation matrix. Moreover, $\mathbf{W}_\ell(\mathbf{k}_\alpha)$ acts only on channel dimensions and is shared across all m components within a fixed degree. It therefore commutes with the Wigner-$D^{(\ell)}$ action. Consequently, both $\mathbf{s}_\alpha^{(\ell)}$ and $\mathbf{M}_i^{(\ell)}$ transform as degree-ℓ features. Although the notation above uses complex exponentials, the implementation uses real cosine and sine accumulations; with symmetric reciprocal sampling and real filters, the final messages are real-valued. These conditions hold for the periodic implementation under a rigid co-rotation of the cell and atomic coordinates. A fixed finite Cartesian grid used for aperiodic structures is not closed under arbitrary rotations and therefore yields an approximate, resolution-dependent realization of the continuous equivariant operator. We will give more explanations in the following section.

Periodic systems. For periodic systems, the frequency set in Eq. (8) is determined by the supercell. Let $(\mathbf{a}_1, \mathbf{a}_2, \mathbf{a}_3) \in \mathbb{R}^3$ be the supercell lattice vectors and $(\mathbf{b}_1, \mathbf{b}_2, \mathbf{b}_3)$ the corresponding reciprocal lattice vectors satisfying $\mathbf{b}_i \mathbf{a}_j = 2\pi\delta_{ij}$. With $V = \mathbf{a}_1 \cdot (\mathbf{a}_2 \times \mathbf{a}_3)$, the reciprocal lattice vectors are

$$\mathbf{b}_1 = \tfrac{2\pi}{V}(\mathbf{a}_2 \times \mathbf{a}_3), \quad \mathbf{b}_2 = \tfrac{2\pi}{V}(\mathbf{a}_3 \times \mathbf{a}_1), \quad \mathbf{b}_3 = \tfrac{2\pi}{V}(\mathbf{a}_1 \times \mathbf{a}_2). \tag{12}$$

Here $\mathbf{a}_i$ are the supercell lattice vectors, $\mathbf{b}_i$ are the reciprocal lattice vectors, δ_{ij} is the Kronecker delta, and V is the supercell volume.

Following EwaldMP, we truncate Fourier frequency sampling by an index box rather than selecting all reciprocal lattice frequencies inside a fixed cutoff volume, which keeps the number of sampled frequencies fixed across structures. We consider integer triples

$$(n_x, n_y, n_z) \in \mathcal{I} = \{-N_x, \ldots, N_x\} \times \{-N_y, \ldots, N_y\} \times \{-N_z, \ldots, N_z\}, \tag{13}$$

and form reciprocal vectors

$$\mathbf{k}_{n_x,n_y,n_z} = n_x\mathbf{b}_1 + n_y\mathbf{b}_2 + n_z\mathbf{b}_3. \tag{14}$$

Here $\mathcal{I}$ is the integer index box, (n_x, n_y, n_z) is one frequency grid index, and N_x, N_y, N_z control the number of frequencies along the three reciprocal-basis directions. The vector $\mathbf{k}_{n_x,n_y,n_z}$ is the reciprocal lattice frequency associated with this index triple. The resulting set is enumerated as $\{\mathbf{k}_\alpha\}_{\alpha=1}^{N_k}$. Because the structure factors are evaluated directly on reciprocal lattice frequencies, no voxel window is required and $\omega_\Delta(\mathbf{k}, \mathbf{r}) = 1$.

This construction is compatible with rotations of the full periodic structure. If the cell is rotated by R, then $\mathbf{a}_i \mapsto R\mathbf{a}_i$ and the reciprocal basis satisfies $\mathbf{b}_i \mapsto R\mathbf{b}_i$ because $(R\mathbf{b}_i)^\top (R\mathbf{a}_j) = \mathbf{b}_i^\top \mathbf{a}_j$. Therefore each reciprocal vector co-rotates with the atoms and the phase remains unchanged.

In our periodic branch, the frequency filter is a k-independent channel mixer. In our implementation this mixer is shared across degrees:

$$\widetilde{\mathbf{s}}^{(\ell)}_{\alpha,m} = \mathbf{W}^{\mathrm{pbc}}\, \mathbf{s}^{(\ell)}_{\alpha,m}, \qquad \mathbf{W}^{\mathrm{pbc}} \in \mathbb{R}^{C\times C}, \tag{15}$$

where $\mathbf{W}^{\mathrm{pbc}}$ is the periodic branch channel-mixing matrix. Equivariance requires that, for each fixed ℓ, the same channel operation be applied to all m components. We parameterize $\mathbf{W}^{\mathrm{pbc}}$ in a bottleneck form

$$\mathbf{W}^{\mathrm{pbc}} = \mathbf{W}_{\mathrm{up}}\mathbf{W}_{\mathrm{down}}, \qquad \mathbf{W}_{\mathrm{down}} \in \mathbb{R}^{C_\downarrow \times C}, \;\; \mathbf{W}_{\mathrm{up}} \in \mathbb{R}^{C\times C_\downarrow}. \tag{16}$$

Here $\mathbf{W}_{\mathrm{down}}$ maps C channels to a bottleneck dimension $C_\downarrow$, and $\mathbf{W}_{\mathrm{up}}$ maps the bottleneck representation back to C channels. The bottleneck dimension $C_\downarrow$ reduces the parameter count relative to a full $C\times C$ matrix while retaining a learnable channel-mixing operation in the Fourier space branch.

Aperiodic systems. For aperiodic systems, no reciprocal lattice is specified by boundary conditions. Following EwaldMP [35], we therefore regard the structure factor as a function over Fourier space and approximate it by a finite set of coefficients on a cutoff domain. Given a discretization parameter Δk and a frequency cutoff $k_{\max}$, we define

$$\mathcal{I}_\Delta = \left\{\mathbf{n} \in \mathbb{Z}^3 : \|\Delta k\, \mathbf{n}\| \le k_{\max}\right\}, \qquad \{\mathbf{k}_\alpha\}_{\alpha=1}^{N_k} = \{\Delta k\, \mathbf{n} : \mathbf{n} \in \mathcal{I}_\Delta\}. \tag{17}$$

Here Δk controls the Fourier space discretization, $k_{\max}$ defines the cutoff domain, and $N_k = |\mathcal{I}_\Delta|$ is the number of frequency vectors used in the approximation.

The corresponding structure factor coefficients are computed analogously to the periodic case, except that the reciprocal lattice frequencies are replaced by the discretized Fourier space frequencies:

$$\mathbf{s}^{(\ell)}_{\alpha,m} = \sum_j \mathbf{x}^{(\ell)}_{j,m} \exp\left(-\mathrm{i}\, \mathbf{k}_\alpha^\top \mathbf{r}_j\right). \tag{18}$$

More generally, this can be interpreted as projecting the continuous Fourier space structure factor onto a finite set of basis functions, as in the aperiodic formulation of EwaldMP. When a voxel-basis discretization is used, the exponential phase is multiplied by the Fourier transform of the voxel window; we absorb this optional discretization factor into the definition of the coefficient computation.

The aperiodic branch uses a frequency-dependent diagonal channel filter rather than a single frequency-independent mixer. Each frequency vector is embedded through a radial basis $\psi(\|\mathbf{k}_\alpha\|)$ and passed through a bottleneck network to produce channel-wise filter coefficients,

$$\mathbf{f}_\alpha = \mathbf{W}_{\mathrm{up}}\left(\mathbf{W}_{\mathrm{down}}\, \psi(\|\mathbf{k}_\alpha\|)\right) \in \mathbb{R}^C, \tag{19}$$

where $\psi(\|\mathbf{k}_\alpha\|) \in \mathbb{R}^{C_\psi}$ is a fixed radial embedding, and $\mathbf{W}_{\text{down}} \in \mathbb{R}^{C_\downarrow \times C_\psi}$ and $\mathbf{W}_{\text{up}} \in \mathbb{R}^{C \times C_\downarrow}$ are learnable projections. The filter applied to the structure factor channels is

$$\mathbf{W}_\ell(\mathbf{k}_\alpha) = \operatorname{diag}(\mathbf{f}_\alpha). \tag{20}$$

For equivariance, this channel-wise operation is applied identically to all m components within a fixed degree ℓ. Since $\psi(\|\mathbf{k}_\alpha\|)$ depends only on the chosen Fourier space discretization, these radial embeddings can be precomputed and reused.

The Fourier space domain defined by $\|\mathbf{k}\| \le k_{\max}$ is rotationally invariant. However its finite Cartesian sampling is only approximately compatible with arbitrary three-dimensional rotations, because a rotated wave vector does not necessarily coincide exactly with another sampled point. Consequently, the aperiodic implementation is approximately SO(3)-equivariant, with a resolution-dependent error introduced by the Fourier space discretization. The degree-wise feature operations remain consistent with the corresponding irreducible transformation laws.

Atom-wise long-range update. After the filtered structure factors are mapped back to atomic positions, the Fourier-space branch produces real-valued long-range messages

$$\mathbf{M}_{i,m}^{(\ell),t} \in \mathbb{R}^C, \qquad m = -\ell, \dots, \ell.$$

We collect these components into the degree-ℓ feature block

$$\mathbf{M}_i^{(\ell),t} = [\mathbf{M}_{i,m}^{(\ell),t}]_{m=-\ell}^{\ell}.$$

We first apply a degree-specific channel map,

$$\mathbf{U}_{i,m}^{(\ell),t} = \eta\, \mathbf{A}_\ell \mathbf{M}_{i,m}^{(\ell),t}, \qquad \mathbf{A}_\ell \in \mathbb{R}^{C \times C}, \tag{21}$$

where η is a fixed normalization factor. The same matrix $\mathbf{A}_\ell$ is applied to every m component within degree ℓ, as required for $SO(3)$ equivariance.

For $\ell > 0$, the projected messages are modulated by channel-wise gates computed from the scalar feature block of the current atomic representation:

$$\mathbf{g}_i^{(\ell),t} = \sigma\Big(\mathbf{W}_g^{(\ell)} \mathbf{x}_i^{(0),t}\Big) \in \mathbb{R}^C, \qquad \mathbf{W}_g^{(\ell)} \in \mathbb{R}^{C \times C}. \tag{22}$$

The resulting long-range update is

$$\mathbf{x}_{i,m}^{\text{Ewald},(\ell),t} = \begin{cases} \mathbf{U}_i^{(0),t}, & \ell = 0, \\ \mathbf{g}_i^{(\ell),t} \odot \mathbf{U}_{i,m}^{(\ell),t}, & \ell > 0, \end{cases} \tag{23}$$

where $\odot$ denotes channel-wise multiplication. For each $\ell > 0$, the same invariant gate is applied to all m components.

Information fusion. At interaction layer t, the running representation, local update, and long-range reciprocal update are fused by a normalized residual sum,

$$\mathbf{x}_i^{t+1} = \frac{1}{\sqrt{3}} \left(\mathbf{x}_i^t + \mathbf{x}_i^{\mathrm{Local},t} + \mathbf{x}_i^{\mathrm{Ewald},t} \right). \tag{24}$$

Here $\mathbf{x}_i^t$ is the input representation at layer t, $\mathbf{x}_i^{\mathrm{Local},t}$ is the local message-passing update, $\mathbf{x}_i^{\mathrm{Ewald},t}$ is the reciprocal space long-range update, and $1/\sqrt{3}$ keeps the residual variance approximately normalized when summing three branches. The reciprocal update scales as $\mathcal{O}(N_{\mathrm{at}} N_k)$, where N_{at} is the number of atoms and N_k is the number of retained Fourier frequencies. This gives every atom access to global structural information at linear cost in the number of atoms for fixed frequency resolution.

4.2 Training settings

The model is optimized using a loss with energy E and atom-wise forces $\mathbf{F}_i$:

$$\mathcal{L} = \lambda_E \left\| E^{\mathrm{pred}} - E^{\mathrm{ref}} \right\|_1 + \lambda_F \frac{1}{3N} \sum_{i=1}^{N} \left\| \mathbf{F}_i^{\mathrm{pred}} - \mathbf{F}_i^{\mathrm{ref}} \right\|_1, \tag{25}$$

where $\| \cdot \|_1$ denotes the mean absolute error (MAE), E^{pred} and E^{ref} are the predicted and reference total energies per configuration, $\mathbf{F}_i^{\mathrm{pred}}, \mathbf{F}_i^{\mathrm{ref}} \in \mathbb{R}^3$ are the predicted and reference forces on atom i, N is the number of atoms in the configuration, and the factor $1/(3N)$ averages the force MAE over all $3N$ Cartesian components. $\lambda_E, \lambda_F > 0$ are scalar weights balancing the two objectives.

The training settings on the OC20 periodic systems dataset are as follows: a cutoff radius of 6.0Åis used to construct local neighborhood graphs. For Fourier space settings, we followed [35]. In Fourier space, the number of included frequencies along the three lattice directions is adjusted to account for the average anisotropy of the supercell. Observing that the average reciprocal space supercell on OC20 is approximately three times narrower along the surface normal (z-direction) than along the x and y directions, we set 1, 1, and 3 for each direction. In the loss function, the weighting coefficients for energy and forces are set to $\lambda_E = 1$ and $\lambda_F = 100$. On the Molten NaCl dataset, we use a cutoff radius of 5.29,Åand likewise set the numbers of Fourier frequencies along the three lattice directions to 1, 1, and 3. The energy and force loss weights are also set to $\lambda_E = 1$ and $\lambda_F = 100$, respectively. For aperiodic systems, the following settings are employed. The spherical harmonic degree is set to $\ell_{\max} = 3$, and the Ewald-based long-range module uses a frequency cutoff of 0.6Å^{-1}, a voxel resolution of 0.2Å^{-1}, and 128-dimensional Gaussian radial-basis functions to parameterize the frequency-domain filters. The loss-function weighting between energy and forces is fixed at $\lambda_E = 1$ and $\lambda_F = 100$. Additional experimental hyperparameters are provided in Supplementary Tables S1–S5.

Data availability

The datasets used in this work are available at Code Ocean.

Code availability

The source code for reproducing the findings in this paper is available at Code Ocean. It is licensed under the `Apache License 2.0`, which allows users to use, modify, and distribute the code freely, provided that proper attribution is given to the original authors. This open source approach improves the reproducibility of our results and facilitates further research in this area.

References

[1] Hospital, A., Goñi, J.R., Orozco, M., Gelpí, J.L.: Molecular dynamics simulations: advances and applications. Advances and Applications in Bioinformatics and Chemistry, 37–47 (2015)

[2] Senftle, T.P., Hong, S., Islam, M.M., Kylasa, S.B., Zheng, Y., Shin, Y.K., Junkermeier, C., Engel-Herbert, R., Janik, M.J., Aktulga, H.M., *et al.*: The reaxff reactive force-field: development, applications and future directions. npj Computational Materials **2**(1), 1–14 (2016)

[3] Karplus, M., Petsko, G.A.: Molecular dynamics simulations in biology. Nature **347**(6294), 631–639 (1990)

[4] Yao, N., Chen, X., Fu, Z.-H., Zhang, Q.: Applying classical, ab initio, and machine-learning molecular dynamics simulations to the liquid electrolyte for rechargeable batteries. Chemical Reviews **122**(12), 10970–11021 (2022)

[5] Zitnick, L., Das, A., Kolluru, A., Lan, J., Shuaibi, M., Sriram, A., Ulissi, Z., Wood, B.: Spherical channels for modeling atomic interactions. Advances in Neural Information Processing Systems **35**, 8054–8067 (2022)

[6] Geerlings, P., De Proft, F., Langenaeker, W.: Conceptual density functional theory. Chemical reviews **103**(5), 1793–1874 (2003)

[7] Deringer, V.L., Bartók, A.P., Bernstein, N., Wilkins, D.M., Ceriotti, M., Csányi, G.: Gaussian process regression for materials and molecules. Chemical reviews **121**(16), 10073–10141 (2021)

[8] Ramprasad, R., Batra, R., Pilania, G., Mannodi-Kanakkithodi, A., Kim, C.: Machine learning in materials informatics: recent applications and prospects. npj Computational Materials **3**(1), 54 (2017)

[9] Butler, K.T., Davies, D.W., Cartwright, H., Isayev, O., Walsh, A.: Machine learning for molecular and materials science. Nature **559**(7715), 547–555 (2018)

[10] Gubernatis, J., Lookman, T.: Machine learning in materials design and discovery: Examples from the present and suggestions for the future. Physical Review Materials **2**(12), 120301 (2018)

[11] Unke, O.T., Chmiela, S., Sauceda, H.E., Gastegger, M., Poltavsky, I., Schutt, K.T., Tkatchenko, A., Muller, K.-R.: Machine learning force fields. Chemical Reviews **121**(16), 10142–10186 (2021)

[12] Carleo, G., Cirac, I., Cranmer, K., Daudet, L., Schuld, M., Tishby, N., Vogt-Maranto, L., Zdeborová, L.: Machine learning and the physical sciences. Reviews of Modern Physics **91**(4), 045002 (2019)

[13] Batzner, S., Musaelian, A., Sun, L., Geiger, M., Mailoa, J.P., Kornbluth, M., Molinari, N., Smidt, T.E., Kozinsky, B.: E (3)-equivariant graph neural networks for data-efficient and accurate interatomic potentials. Nature communications **13**(1), 2453 (2022)

[14] Musaelian, A., Batzner, S., Johansson, A., Sun, L., Owen, C.J., Kornbluth, M., Kozinsky, B.: Learning local equivariant representations for large-scale atomistic dynamics. Nature Communications **14**(1), 579 (2023)

[15] Batatia, I., Kovacs, D.P., Simm, G., Ortner, C., Csányi, G.: Mace: Higher order equivariant message passing neural networks for fast and accurate force fields. Advances in neural information processing systems **35**, 11423–11436 (2022)

[16] Anstine, D.M., Isayev, O.: Machine learning interatomic potentials and long-range physics. The Journal of Physical Chemistry A **127**(11), 2417–2431 (2023)

[17] Schütt, K.T., Sauceda, H.E., Kindermans, P.-J., Tkatchenko, A., Müller, K.-R.: Schnet–a deep learning architecture for molecules and materials. The Journal of chemical physics **148**(24) (2018)

[18] Gasteiger, J., Groß, J., Günnemann, S.: Directional message passing for molecular graphs. arXiv preprint arXiv:2003.03123 (2020)

[19] Levin, Y.: Polarizable ions at interfaces. Physical review letters **102**(14), 147803 (2009)

[20] Bedrov, D., Piquemal, J.-P., Borodin, O., MacKerell Jr, A.D., Roux, B., Schr"o"der, C.: Molecular dynamics simulations of ionic liquids and electrolytes using polarizable force fields. Chemical reviews **119**(13), 7940–7995 (2019)

[21] Borodin, O.: Polarizable force field development and molecular dynamics simulations of ionic liquids. The Journal of Physical Chemistry B **113**(33), 11463–11478 (2009)

[22] Cheng, B.: Latent ewald summation for machine learning of long-range interactions. npj Computational Materials **11**(1), 80 (2025)

[23] Gao, R., Yam, C., Mao, J., Chen, S., Chen, G., Hu, Z.: A foundation machine learning potential with polarizable long-range interactions for materials modelling. Nature Communications **16**(1), 10484 (2025)

[24] Huguenin-Dumittan, K.K., Loche, P., Haoran, N., Ceriotti, M.: Physics-inspired equivariant descriptors of nonbonded interactions. The Journal of Physical Chemistry Letters **14**(43), 9612–9618 (2023)

[25] Niblett, S.P., Galib, M., Limmer, D.T.: Learning intermolecular forces at liquid–vapor interfaces. The Journal of chemical physics **155**(16) (2021)

[26] Unke, O.T., Chmiela, S., Gastegger, M., Schütt, K.T., Sauceda, H.E., Müller, K.-R.: Spookynet: Learning force fields with electronic degrees of freedom and nonlocal effects. Nature communications **12**(1), 7273 (2021)

[27] Unke, O.T., Meuwly, M.: Physnet: A neural network for predicting energies, forces, dipole moments, and partial charges. Journal of chemical theory and computation **15**(6), 3678–3693 (2019)

[28] Ko, T.W., Finkler, J.A., Goedecker, S., Behler, J.: A fourth-generation high-dimensional neural network potential with accurate electrostatics including non-local charge transfer. Nature communications **12**(1), 398 (2021)

[29] Gao, A., Remsing, R.C.: Self-consistent determination of long-range electrostatics in neural network potentials. Nature communications **13**(1), 1572 (2022)

[30] Shaidu, Y., Pellegrini, F., Küçükbenli, E., Lot, R., Gironcoli, S.: Incorporating long-range electrostatics in neural network potentials via variational charge equilibration from shortsighted ingredients. npj Computational Materials **10**(1), 47 (2024)

[31] Zhang, L., Wang, H., Muniz, M.C., Panagiotopoulos, A.Z., Car, R., et al.: A deep potential model with long-range electrostatic interactions. The Journal of Chemical Physics **156**(12) (2022)

[32] Schütt, K., Kindermans, P.-J., Sauceda Felix, H.E., Chmiela, S., Tkatchenko, A., Müller, K.-R.: Schnet: A continuous-filter convolutional neural network for modeling quantum interactions. Advances in neural information processing systems **30** (2017)

[33] Deng, B., Zhong, P., Jun, K., Riebesell, J., Han, K., Bartel, C.J., Ceder, G.: Chgnet as a pretrained universal neural network potential for charge-informed atomistic modelling. Nature Machine Intelligence **5**(9), 1031–1041 (2023)

[34] Yu, H., Hong, L., Chen, S., Gong, X., Xiang, H.: Capturing long-range interaction with reciprocal space neural network. arXiv preprint arXiv:2211.16684 (2022)

[35] Kosmala, A., Gasteiger, J., Gao, N., Günnemann, S.: Ewald-based long-range message passing for molecular graphs. In: International Conference on Machine Learning, pp. 17544–17563 (2023). PMLR

[36] King, D.S., Kim, D., Zhong, P., Cheng, B.: Machine learning of charges and long-range interactions from energies and forces. Nature Communications **16**(1), 8763 (2025)

[37] Grisafi, A., Ceriotti, M.: Incorporating long-range physics in atomic-scale machine learning. The Journal of chemical physics **151**(20) (2019)

[38] Duval, A., Mathis, S.V., Joshi, C.K., Schmidt, V., Miret, S., Malliaros, F.D., Cohen, T., Lio, P., Bengio, Y., Bronstein, M.: A hitchhiker's guide to geometric gnns for 3d atomic systems. arXiv preprint arXiv:2312.07511 (2023)

[39] Thomas, N., Smidt, T., Kearnes, S., Yang, L., Li, L., Kohlhoff, K., Riley, P.: Tensor field networks: Rotation-and translation-equivariant neural networks for 3d point clouds. arXiv preprint arXiv:1802.08219 (2018)

[40] Geiger, M., Smidt, T.: e3nn: Euclidean neural networks. arXiv preprint arXiv:2207.09453 (2022)

[41] Passaro, S., Zitnick, C.L.: Reducing so (3) convolutions to so (2) for efficient equivariant gnns. In: International Conference on Machine Learning, pp. 27420–27438 (2023). PMLR

[42] Liao, Y.-L., Wood, B., Das, A., Smidt, T.: Equiformerv2: Improved equivariant transformer for scaling to higher-degree representations. arXiv preprint arXiv:2306.12059 (2023)

[43] Wang, T., He, X., Li, M., Shao, B., Liu, T.-Y.: Aimd-chig: Exploring the conformational space of a 166-atom protein chignolin with ab initio molecular dynamics. Scientific Data **10**(1), 549 (2023)

[44] Faller, C., Kaltak, M., Kresse, G.: Density-based long-range electrostatic descriptors for machine learning force fields. The Journal of Chemical Physics **161**(21) (2024)

[45] Chanussot, L., Das, A., Goyal, S., Lavril, T., Shuaibi, M., Riviere, M., Tran, K., Heras-Domingo, J., Ho, C., Hu, W., *et al.*: Open catalyst 2020 (oc20) dataset and community challenges. Acs Catalysis **11**(10), 6059–6072 (2021)

[46] Ji, Y., Liang, J., Xu, Z.: Machine-learning interatomic potentials for long-range systems. Phys. Rev. Lett. **135**, 178001 (2025) https://doi.org/10.1103/ssp9-7s81

[47] Wang, T., He, X., Li, M., Li, Y., Bi, R., Wang, Y., Cheng, C., Shen, X., Meng, J., Zhang, H., *et al.*: Ab initio characterization of protein molecular dynamics with ai2bmd. Nature **635**(8040), 1019–1027 (2024)

Supplementary Files

This is a list of supplementary files associated with this preprint. Click to download.

- sup.pdf